From the micromechanics of Darcy's law to particle-laden flows in porous media

Gamaliel Jeevan Dewanto[1,*], *Jack* Widjajakusuma[2], and *Hans-Georg* Matuttis[1]

[1]Department of Mechanical and Intelligent Systems Engineering, The University of Electro-Communications, Japan
[2]Department of Civil Engineering, Pelita Harapan University, Indonesia

Abstract. We simulate flow in porous media using a two-dimensional combination of a DEM method (for the solid particles) and a FEM method (for the fluid). The fluid properties correspond to those of water, and porous domains are constructed by embedding fixed polygonal particles within a flow channel. By extracting subsamples of increasing size from a larger porous domain, we find a clear convergence from micro-geometry dependence to bulk behavior. This identifies the size of the Representative Elementary Volume (REV) of approximately 20 times the maximum particle diameter. We compare a disordered granular configuration with ordered square and staggered grid arrangements, all having the same porosity. The ordered systems exhibit higher permeability and more regular flow patterns, demonstrating the strong influence of pore structure on macroscopic flow. Our findings support the application of Darcy's law for estimating pressure boundary conditions. This provides a basis for improving stability in future time-dependent simulations involving moving particles and evolving porous structures.

1 Introduction

We simulate flow in a porous medium using a combination of Finite Element Method (FEM) for the fluid and Discrete Element Method (DEM) for the solid particles. Our previous findings from pipe flow simulations suggest that defining both velocity and pressure boundary conditions enhances the stability of the simulation, provided that the velocity and pressure values are appropriately matched. Their adjustment is crucial for maintaining stability, especially in porous flow scenarios due to the inherent complexities of fluid-particle interactions and flow characteristics. This approach will become even more important when we have free-moving particles colliding within the porous flow and generating high-pressure gradients, which can cause instabilities. Further discussion on boundary condition formulation and their effects on stability can be found in Section 3. For pipe flow, we use the Darcy-Weisbach equation to establish the relationship between pressure change and flow rate based on the channel geometry. This equation is given by:

$$\frac{\Delta p}{L} = \frac{24}{Re} \cdot \frac{\rho}{2D} \cdot v. \tag{1}$$

Here, Δp is the pressure drop over a length L, Re is the Reynolds number, ρ is the fluid density, D is the channel width and v is the average velocity. The equation shows the pressure drop is inversely proportional to the channel width, D. However, in porous media flow, the relation shifts from being dependent on channel width to being governed by the permeability of the porous medium, as expressed by Darcy's law:

$$v = -\frac{K}{\mu} \cdot \frac{\Delta p}{L}. \tag{2}$$

In this equation, K represents the intrinsic permeability of the medium, influenced by porosity, particle angularity, and void connectivity, while μ is the fluid's dynamic viscosity. Unlike in pipe flow, where velocity depends on channel width, Darcy's law highlights permeability as the primary resistance in porous media. This raises an important question: when does the dominant flow behavior shift from being governed by the pore-scale geometry to being effectively described by bulk properties such as permeability? In our study, this transition is investigated by iteratively scaling up the subsamples of a master porous structure. At small domain sizes, fluid motion is strongly influenced by the pore-scale geometry. However, as the domain size increases, the influence of individual pores averages out, and the flow behavior converges toward a representative macroscopic response. This shift—from micro to macro description—is formalized by the Representative Elementary Volume (REV): the minimum volume over which measurements such as permeability become statistically stable and spatially independent. The shift in the dependency is central to our investigation, where we aim to determine how Darcy's law can be applied to formulate the correct velocity-pressure pair for the boundary conditions. Furthermore, we explore how varying particle arrangements influence flow properties and stability. Our FEM implementation discretizes the fluid domain into triangular elements, employing a $P_2^+P_1$ scheme: velocity com-

*e-mail: jeevan.dewanto@gmail.com

© The Authors, published by EDP Sciences. This is an open access article distributed under the terms of the Creative Commons Attribution License 4.0 (https://creativecommons.org/licenses/by/4.0/).

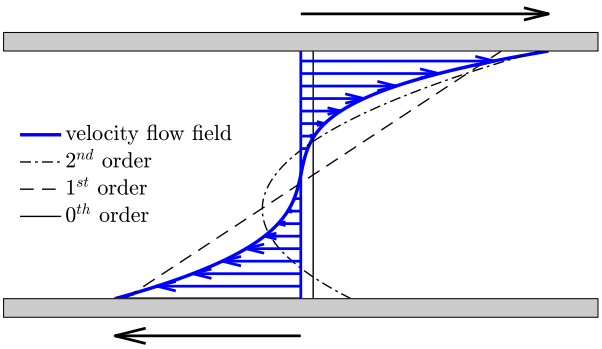

Figure 1. Horizontal velocity flow field between two moving boundaries (top and bottom plates moving in opposite directions according to the arrows) require higher-order polynomials (blue line, at least of effective order 3) to satisfy the curvature of the flow field, lower-order polynomials lead to unsatisfying approximations.

ponents are stored as second-order polynomials with an embedded bubble function (effectively third-order), while pressure components are stored as first-order polynomials [1]. This satisfies the Ladyzhenskaya–Babuška–Brezzi stability condition and allows the stable and accurate resolution of complex flow profiles (as in Fig. 1) in confined porous spaces without the computational cost of higher-order elements. The porous medium is modeled using a DEM with polygon [2], allowing seamless integration into the triangular FEM-grid. The polygonal boundaries of the DEM elements serve as boundaries for FEM computations, and fluid-particle interactions are computed as surface integrals as the form drag and the friction drag. In 2D fluid simulations, closely packed particles can create discontinuities, isolating fluid regions. To address this, we introduce a "core and shadow" approach, where the effective particle boundary is offset inward to form a permeable outline we refer as the "shadow" allowing fluid passage through between connected particles (see Fig. 2).

2 Porous Medium Construction

We construct the porous medium by randomly placing polygonal particles of varying sizes within a 30×30 mm domain. The particle diameters ranges from 0.125 mm to 0.5 mm, comparable to fine-grain sand. The resulting geometry consists of about 14000 particles and has a porosity of $\phi = 0.435$. From this geometry, we can cut sections of subsamples out of this master geometry to put into a flow channel. We tested different sizes of subsamples taken

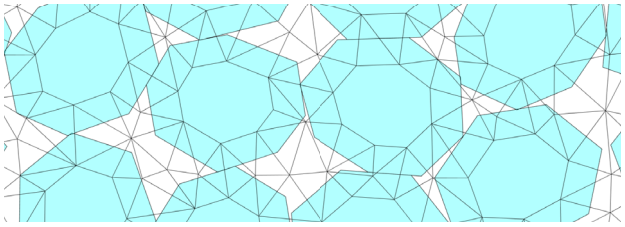

Figure 2. Connected polygonal particles with shadows bridging otherwise isolated fluid domains.

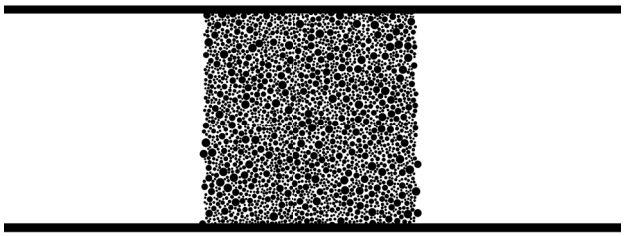

Figure 3. A 12×12 mm subsample of the master 30×30 mm porous medium (made from regular polygons with 20 to 80 corners) inserted into the middle of a flow channel. Fluid flows from the inflow (left) to the outflow (right).

from different sections of the master configuration. Fig. 3 shows a 12×12 mm subsample placed inside a flow channel. In addition to this porous medium, we construct two more configurations with the same porosity: (1) uniformly sized particles placed on a square grid and (2) uniformly sized particles placed on a staggered grid. These configurations allow us to examine the effect of ordered versus disordered arrangements on permeability and flow stability. To prevent preferential flow in the region along the smooth boundary walls, we arrange a partial overlap between the outermost particles and the channel boundaries, effectively integrating the particles into upper and lower boundary wall.

3 Pressure Boundary Condition

Gresho and Sani [3] recommend to understand the FEM as a least squares fit of piecewise polynomials to the underlying partial differential equations and the boundary conditions. In general, for channel flow of pure fluids, parallel velocities at the inflow are sufficient to hoist up the flow field over the whole system domain to physical values, at least for Reynolds numbers < 100. Setting boundary conditions at the outflow is usually not very useful, as vortices may form in e.g., the flow around obstacles inside the system, which are then transported to the outflow region and contradict the outflow velocity conditions. In this case, the simulation usually “locks”, i.e. crashes, because no “fit” of the velocities close to the boundary (vortices) and on the boundary (parallel outflow) can be found. While inflow velocity conditions are sufficient for pure fluids, the situation changes when moving particles are present in the simulation. On the one hand, particles may have to be first accelerated to velocities which are consistent with the surrounding flow field. In this case, the velocity conditions on the particle boundaries may be at odds with those at the inflow, and if there are boundary points on many particles (proportional to the area of the domain) and few points at the inflow (proportional to the cross section), spurious flow fields may result until the simulation also “locks” for this case. Another danger, for particle-laden flow in a porous medium, are collisions between floating particles and those of the surrounding fixed granular matrix: If the pressure field is only built up due to the inflow velocity boundary conditions, it is relatively weak against perturbations. Ricocheting of free particles from the fixed

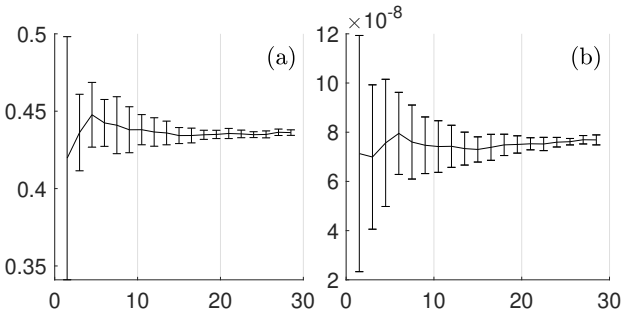

Figure 4. Average porosity (a) and permeability (b) with their respective standard deviations for four non-overlapping subsamples. The non-averaged porosities converged faster than the non-averaged permeabilities.

granular matrix may become a rather severe perturbation, which may distort the global pressure field and destabilize the simulation. In that case, with particles coliding with the granular matrix at low Reynolds numbers, the flow becomes highly variable and unstable, while for pure Newtonian fluids, the flow through the same porous geometry is hydrodynamically the simplest, numerically most stable case. In the logic of FEM-simulations in terms of least squares fits, this motivates the increase of the number of boundary conditions, in particular of setting additional pressure boundary conditions at the inflow. For the outflow, it would be enough to define the pressure only at a single point on the boundary so that the pressure gradient becomes effective to control the pressure field in the flow domain. Such a point with pressure $p = 0$ is usually defined anyway as the reference pressure, to prevent the drift of the pressure field during iterations. In that case, the question is the "correct" magnitude of this "reference pressure", i.e. a pressure which exactly maintains the flow consistent with the inflow velocity boundary condition. Inconsistency of the velocity- and pressure-boundary conditions would be reflected in an incrase of the condition number of the Jacobian, in the same way as the condition number for the linear system in a least squares fit increases for increasingly inconsistent input data. A natural choice for the computation of the gauge pressure seems to be based on the Bernoulli equation with the gravity g

$$\frac{v^2}{2} + gh + \frac{p_{\text{gauge}}}{\rho} = 0 \tag{3}$$

along height h and a pressure gradient p_{gauge} with fluid density ρ. As we are interested in horizontal flow, we can drop the gravity term and obtain the magnitude of the gauge pressure gradient (scaled in density) as

$$\left|\frac{\Delta p_{\text{gauge}}}{\rho}\right| = \frac{v^2}{2}. \tag{4}$$

Unfortunately, the Bernoulli equation (see Eq. 3) is essentially an energy conservation equation which is valid parallel, but not (in the presence of viscosity) normal to the flow lines. This means that equation 4 could be used for the Euler equation of fluid dynamics, but not for the Navier Stokes equation. As a result, we chose the boundary condition using a defined pressure difference between the inflow and outflow, ΔP. The FEM will then compute the "correct" stationary flow velocity corresponding to ΔP, which is enforced as the inflow boundary condition during the time evolution steps, along with the pressure. The rationale for selecting a defined pressure instead of a velocity stems from experimental practices: in most experiments measuring permeability in porous media, pressure is the independent variable, while the flow rate (or velocity) is the measured quantity.

4 Results

The porosity and permeability were computed by resampling—iteratively sized subsamples of the 30×30 mm master configuration. Subsample sized from $1.5d_{max}$ to $30d_{max}$, with the maximum particle diameter d_{max}. Porosity was defined as the ratio of void area to the total area, while permeability was obtained by applying a pressure difference of $\Delta P = 0.005$ and measuring the average flow rate. As shown in Figure 4, both properties converge with increasing sample size, though stabilization occurs later for permeability. This indicates that the representative elementary volume (REV) depends on the specific observable, in our case the permeability. To better quantify the REV size, we computed the statistical REV (sREV)—the size below which the statistics (mean and standard deviation) of the measurement vary significantly. Following the criterion as presented in [4] for sREV. Using a stability threshold of $\epsilon = 0.05$, the sREV size for the permeability was determined to be $19.5d_{max}$ (9.75 mm). To investigate how particle arrangement influences flow behaviour and permeability, we compared a 10×10 mm disordered porous medium (a subsample from the master geometry)

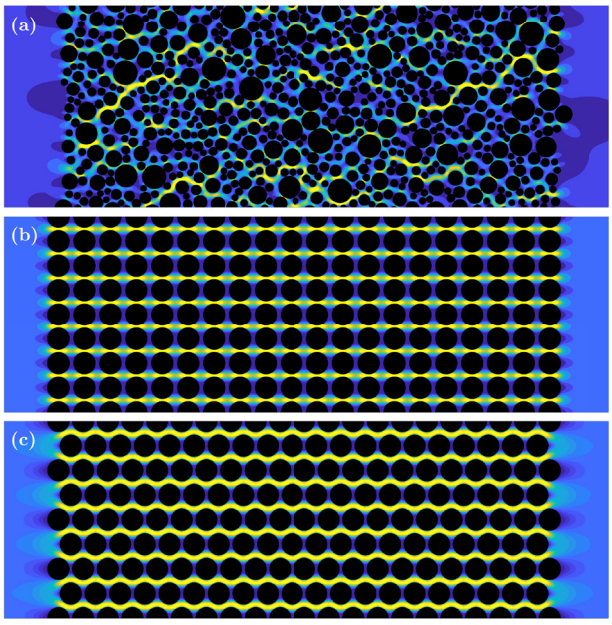

Figure 5. Flow velocity contour of the (a) disordered pore structure, (b) square grid pore structure and (c) staggered grid pore structure. These are 4 mm width strips cropped from each corresponding 10×10 mm porous geometries.

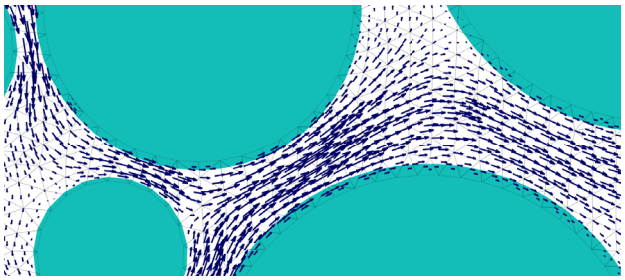

Figure 6. Cut-out of the disordered flow geometry from Fig. 5 with the flow indicated by the arrows: the channel in the upper middle, though wide, carries hardly any flow due to its relative orientation to the general flow direction.

with two ordered configurations: a square grid and a staggered grid of uniformly sized particles, all constructed to have the same porosity ($\phi = 0.435$) and dimension (10×10 mm) as the disordered system. Figure 5 shows the flow field in each configuration. It is visible that while the porosity is the same, the spatial arrangement of particles largely affect the flow behavior, seen based on the pattern. In the disordered medium, the flow field is highly tortuous. Local accelerations and decelerations occur due to the irregular geometry. This heterogeneity results in a lower bulk permeability of $K_{disordered} = 0.0721 \times 10^{-6}$ compared to $K_{square} = 0.2236 \times 10^{-6}$ and $K_{staggered} = 0.5743 \times 10^{-6}$, as the pressure drop must overcome a more intricate resistance network. By contrast, the square and staggered grid configuration produces highly symmetric flow lanes aligned with the geometry. We also observed that the higher permeability in the staggered geometry, $K_{staggered}$, compared to the square geometry, K_{square}, can be attributed to the narrower interstices between obstacles of the square geometry. Additionally, for disordered geometries, it is difficult to infer a clear relationship between the flow rate and the pore geometry. This is because the totality of the pore structure—comprising factors like width, orientation, and size distribution—determines the flow rate. As shown in figure 6, even wide channels may carry less flow than narrower adjacent channels due to differences in orientation and connectivity. In figure 7, one can see that the pressure decay is confined to the range of the porous matrix in the system, outside this range, the pressure gradient is practically zero. This brings to mind the analogy between electrodynamics and hydrodynamics between pressure and voltage: In the same way as voltage drops occur in regions of high electric resistance, the pressure drops occur in regions of large hydrodynamic resistance.

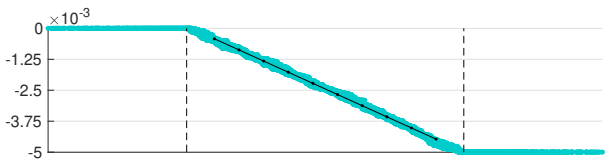

Figure 7. Pressure drop along the flow direction. Light blue dots are the actual pressure values of the FEM elements. The solid line is the trendline of the pressure drop within the porous matrix.

5 Conclusions

Our study investigated the influence of pore structure on flow behavior, particularly in relation to Darcy's law and pressure-driven flow in porous media. By systematically extracting subsamples of increasing size from a larger porous domain, we find a clear convergence from micro-geometry dependence to bulk behavior. This was evidenced for the porosity and the permeability beyond sample sizes of $\approx 20 d_{\max}$. This identifies the Representative Elementary Volume (REV) for our configuration of nearly round polygonal particles with $\phi = 0.435$. Below this REV threshold, the permeability significantly fluctuates due to the dominant disorder of the micro-geometry. Above the REV size, the permeability converges to a value of an intrinsic material property. This has practical implications for the formulation of boundary conditions in time-evolving simulations. While the present study focuses on stationary flow, future dynamic simulations involving freely moving particles will benefit from Darcy-derived pressure estimates and the corresponding combined velocity boundary conditions to improve numerical stability. Our identification of the REV further justifies the use of Darcy's law in estimating pressure values for the boundary conditions, provided the domain size exceeds this threshold. Our results offer evidence for its applicability within a coupled FEM-DEM framework. To better understand the role of pore geometry, we compared the disordered geometry to two ordered configurations: square and staggered grids of uniformly sized particles. Despite the identical porosities, the ordered systems displayed consistently higher permeabilities and regular flow patterns. This highlights that pore connectivity and alignment—not just porosity—play a central role in determining the macroscopic flow behavior. Together, these findings provide a foundation for extending coupled FEM–DEM frameworks to more complex scenarios. Future work will include suspended particles and transient flows to study the effect of particle–fluid interactions on permeability and flow stability in changing geometries.

References

[1] J. Mueller, Ph.D. thesis, The University of Electro-Communications, Department of Mechanical Engineering and Intelligent Systems (2022)

[2] H.G. Matuttis, J. Chen, Understanding the Discrete Element Method (Wiley, 2014)

[3] P. Gresho, R. Sani, Incompressible Flow and the Finite Element Method, Vol. 2 (Wiley, 2000)

[4] A.S. Zubov, A.N. Khlyupin, M.V. Karsanina, K.M. Gerke, In search for representative elementary volume (rev) within heterogeneous materials: A survey of scalar and vector metrics using porous media as an example, Advances in Water Resources **192**, 104762 (2024). https://doi.org/10.1016/j.advwatres.2024.104762